

Effect of water vapor on the structure and stability of self-organized patterns in atmospheric-pressure pulsed radio-frequency dielectric barrier discharges

Man-Qiang Du(杜满强), Wen-Fu Wei(魏文赋), Zhen-Feng Ding(丁振峰), Liang-Wen Qi(漆亮文), Xiao-Dong Wen(温晓东), and Bin Sun(孙斌)

Citation: Chin. Phys. B, 2026, 35 (**3**): 035201. DOI: 10.1088/1674-1056/adf181
http://cpb.iphy.ac.cn; http://iopscience.iop.org/cpb

What follows is a list of articles you may be interested in

Simulation on atmospheric pressure barrier discharge with varying relative position between two wavy dielectric surfaces

Xue-Chen Li(李雪辰), Wen-Jie Wan(万文杰), Xiao-Qian Liu(刘晓倩), Mo Chen(陈墨), Kai-Yue Wu(吴凯玥), Jun-Xia Ran(冉俊霞), Xue-Xia Pang(庞学霞), Xue-Xue Zhang(张雪雪), Jia-Cun Wu(武珈存), Peng-Ying Jia(贾鹏英), and Hui Sun(孙辉)

Chin. Phys. B, 2025, 34 (**3**): 035202. DOI: 10.1088/1674-1056/ada43d

Spatial characteristics of nanosecond pulsed micro-discharges in atmospheric pressure He/H_2O mixture by optical emission spectroscopy

Chuanjie Chen(陈传杰), Zhongqing Fang(方忠庆), Xiaofang Yang(杨晓芳), Yongsheng Fan(樊永胜), Feng Zhou(周锋), and Rugang Wang(王如刚)

Chin. Phys. B, 2022, 31 (**2**): 025204. DOI: 10.1088/1674-1056/ac2e62

ttenuation characteristics of obliquely incident electromagnetic wave in weakly ionized dusty plasma based on modified Bhatnagar-Gross-Krook collision model

Zhaoying Wang(王召迎), Lixin Guo(郭立新), and Jiangting Li(李江挺)

Chin. Phys. B, 2021, 30 (**4**): 045203. DOI: 10.1088/1674-1056/abe230

Numerical study on the discharge characteristics and nonlinear behaviors of atmospheric pressure coaxial electrode dielectric barrier discharges

Ding-Zong Zhang(张定宗), Yan-Hui Wang(王艳辉), De-Zhen Wang(王德真)

Chin. Phys. B, 2017, 26 (**6**): 065206. DOI: 10.1088/1674-1056/26/6/065206

Atmospheric pressure plasma jet utilizing Ar and Ar/H_2O mixtures and its applications to bacteria inactivation

Cheng Cheng (程诚), Shen Jie (沈洁), Xiao De-Zhi (肖德志), Xie Hong-Bing (谢洪兵), Lan Yan (兰彦), Fang Shi-Dong (方世东), Meng Yue-Dong (孟月东), Chu Paul K (朱剑豪)

Chin. Phys. B, 2014, 23 (**7**): 075204. DOI: 10.1088/1674-1056/23/7/075204

Effect of water vapor on the structure and stability of self-organized patterns in atmospheric-pressure pulsed radio-frequency dielectric barrier discharges

Man-Qiang Du(杜满强)[1,2], Wen-Fu Wei(魏文赋)[3], Zhen-Feng Ding(丁振峰)[4], Liang-Wen Qi(漆亮文)[1], Xiao-Dong Wen(温晓东)[1], and Bin Sun(孙斌)[5,†]

[1] *School of Mathematics and Physics, Lanzhou Jiaotong University, Lanzhou* 730070, *China*
[2] *Gansu Center for Fundamental Research in Complex Systems Analysis and Control, Lanzhou Jiaotong University, Lanzhou* 730070, *China*
[3] *College of Electrical Engineering, Southwest Jiaotong University, Chengdu* 610031, *China*
[4] *School of Physics, Dalian University of Technology, Dalian* 116024, *China*
[5] *School of Mechanics and Aerospace Engineering, Dalian University of Technology, Dalian* 116024, *China*

(Received 29 May 2025; revised manuscript received 4 July 2025; accepted manuscript online 18 July 2025)

The effect of water vapor on the self-organized pattern characteristics of atmospheric-pressure radio-frequency argon dielectric barrier discharges was experimentally investigated. Under high relative humidity (RH) conditions, no side discharges were generated between the two surface discharges of the patterns. As the RH gradually decreases, side discharges begin to emerge and evolve through three distinct modes: uniform glow discharge, non-uniform glow discharge, and filamentary discharge. These structural variations are primarily attributed to changes in breakdown (or maintenance) voltage induced by varying RH. At lower RH levels, the strongest single pattern exhibited spontaneous motion, which in turn triggered the collective motion of patterns. The self-organized pattern motion is explained as the shift of re-ignition position induced by electric interaction between asymmetrical side discharge filaments and the central filament.

Keywords: atmospheric-pressure pulsed radio-frequency (RF) discharges, dielectric barrier discharges, self-organized pattern, water vapor

PACS: 52.25.Mq, 52.30.–q, 52.65.Yy, 52.65.Kj

DOI: 10.1088/1674-1056/adf181 **CSTR:** 32038.14.CPB.adf181

1. Introduction

Atmospheric-pressure plasma sources have garnered significant research interest over recent decades due to their low production cost, easy implementation and applications ranging from surface modification,[1,2] plasma medicine,[3,4] sterilization,[5,6] etc. In alternating current atmospheric-pressure gas discharges, uniform glow discharges are achievable in dielectric barrier discharges (DBDs) whose metal electrodes are covered with an insulating dielectric layer.[7–10] However, introducing dielectric into an atmospheric-pressure low-frequency (several to hundreds of kHz) DBDs does not ensure a uniform glow, but instead, non-uniform discharges in the form of self-organized patterns appear within a certain parameter regime.[11–18] The well-validated physical mechanism underlying pattern formation in low-frequency DBDs is the activation-inhibition effect.[7,19] Specifically, the formation of self-organized patterns originates from the following mechanisms. The reignition of filaments first occurs in regions with the highest surface charge and residual volume charge density during the first half-cycle (i.e., the first activation region).[7] Simultaneously, charges carried by the discharge filaments diffuse along the dielectric surface, creating inhibition regions around them that impede the generation of new discharges in their vicinity. As the voltage amplitude continues to increase within the same half-cycle, weak current side discharges can form at the edges of the inhibition region, known as the second activation region. The properties of these side discharges are strongly dependent on experimental conditions and can explain many aspects of filament interactions, dynamics, and pattern formation.[7] A wide variety of patterns were produced and elucidated in extensive experimental and numerical studies on low-frequency DBDs.[13,15,16] Self-organized patterns are generally stable when their filament number is below a certain threshold. The one reported isolated pattern in low-frequency DBDs is not only stable but also structure-limited, exhibiting only two distinct configurations: filaments and columns.[7,20,21]

The addition of small amounts of molecular gases (e.g., water vapor) to inert gas DBDs enhances plasma reactivity and modifies both the structure and stability of self-organized patterns.[22,23] For both single filament and multi-filament, random filament motion is induced by water vapor desorbed from dielectric surfaces due to heating by the filaments.[23] This phenomenon is attributed to a shift in filament reignition towards regions of lower breakdown voltage, driven by water vapor concentration gradients surrounding the filaments.

[†]Corresponding author. E-mail: sunbin83@dlut.edu.cn

© 2026 Chinese Physical Society and IOP Publishing Ltd. All rights, including for text and data mining, AI training, and similar technologies, are reserved.

When the water vapor is depleted, self-organized patterns cease moving.

Compared to low-frequency DBDs, radio-frequency (RF) DBDs have emerged as a prominent plasma source for generating stable atmospheric-pressure glow discharge.[24–26] This configuration offers dual benefits: reduced breakdown voltage and suppression of arcing discharges. Under atmospheric-pressure continuous-wave RF excitation in pure argon or helium, RF DBDs typically operate in uniform glow discharges.[26,27] However, when nitrogen is introduced into the inert gas, continuous-wave RF DBDs exhibit self-organized patterns.[28–30]

Notably, atmospheric-pressure inert gas continuous-wave RF DBDs operating in high-power γ-mode exhibit elevated gas temperatures, which limit the applicability in processing temperature-sensitive materials.[27] To mitigate gas heating in continuous-wave RF discharges, pulsed RF excitation was proposed,[31,32] and is expected to better maintain uniform glow discharges when combined with dielectric barriers. However, self-organized patterns have been observed in both experiments and numerical simulations of low duty-cycle pulsed RF DBDs,[31,33–35] exhibiting pattern discharges analogous to those in low-frequency DBDs. Recently, the structural characteristics and generation mechanism of patterns in pulsed RF DBDs were experimentally investigated by varying the driving frequency.[35] The results demonstrate that within the low-to-medium driving frequency range (3.0–9.0 MHz), the largest single-pattern cluster consists of a central filament and side discharges (glow or filaments) surrounding the central filament. New filaments are generated via the splitting of the strongest side discharges. In low-frequency DBDs, side discharges not only explain the dynamic behavior of patterns, such as splitting, merging, generation and annihilation, but also elucidate the collective long-range migratory motion of a rotating pair of traveling filaments.[13] Although pulsed RF and low-frequency patterns share the same formation mechanism, their excitation frequencies differ by several orders of magnitude. The use of RF excitation induces electron trapping in the oscillating field, significantly affecting lateral discharges.[36] Simultaneously, during the pulsed RF discharge process, the periodic variation of the RF voltage within a single pulse cycle induces dynamic evolution of the side discharges.[35] Despite systematic studies on frequency effects in pulsed RF DBDs, two issues remain unresolved: (1) how molecular gas content (e.g. water vapor) regulates the self-organized pattern structure, and (2) the stability of these patterns.

In this paper, we report the effect of water vapor on the structure of self-organized patterns in atmospheric-pressure pulsed RF DBDs, and analyze the motion of patterns under low relative humidity (RH) conditions.

2. Experimental setup

The experimental setup is schematically shown in Fig. 1, and the details are described in Ref. [35]. The circular copper electrodes ($\varphi = 60$ mm) were covered with square alumina-sheet (99.999% purity, 80 mm in side length, 0.64 mm in thickness). The gas gap between two alumina sheets was set at 1.0 mm. The discharge electrodes were sealed in an acrylic box, in which the gas pressure was maintained at 760 Torr at an argon gas flow rate of 1.0 L/min. Other discharge parameters are as follows: a driving frequency of 9.0 MHz, a pulse repetition frequency of 10 kHz and a duty ratio of 7%.

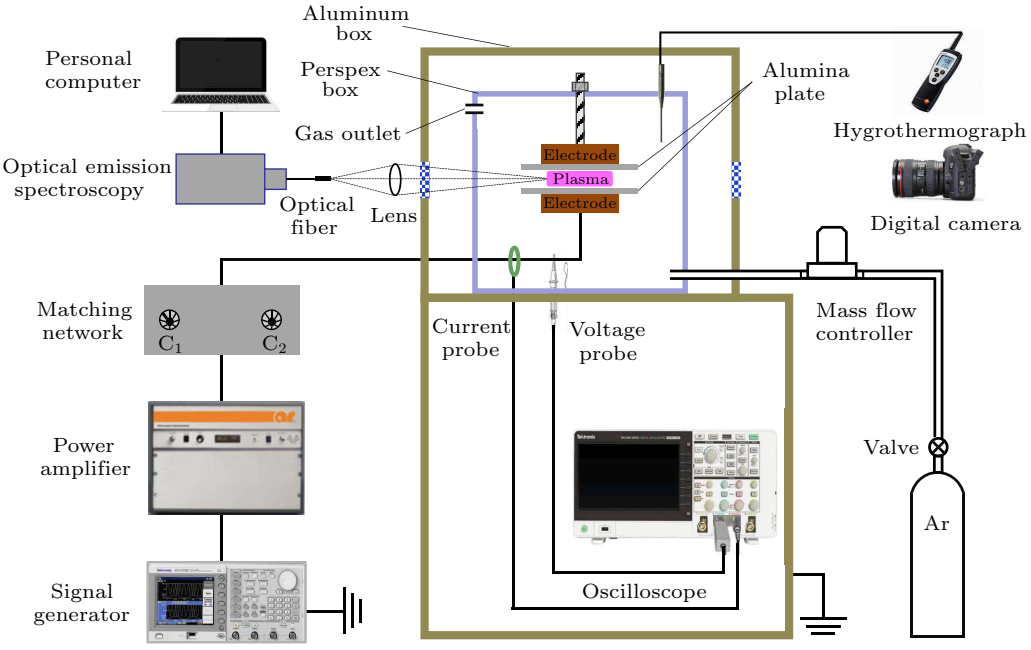


Fig. 1. Experimental setup.

The pulsed driving frequency signal was generated with a signal generator (Tektronix AFG 3102) and then amplified by an amplifier (AR 500A100A). The pulsed RF voltage applied to the electrodes was measured with a voltage probe (Tektronix P6015A). The net pulsed RF power (incident power minus reflected power) was read from the AR amplifier's built-in power meter. Discharge images were recorded from a side view of the electrodes with a Canon camera (EOS 50D) at a shutter speed of 1/100 s, with a lens aperture of F5.6 and an ISO of 3200. The recorded 32-bit RGB (red, green and blue) true-color images in JPEG (joint photographic experts group) format were converted to 32-bit grayscale (0 to 255 scale) files by the image processing software ImageJ using the average method, enabling the numerical analysis of the radial plasma profiles in the discharge image. Gray value analysis of discharge images has been shown to be an effective method for determining the intensity and uniformity of plasma at atmospheric-pressure discharges.[37] Water vapor in the air could penetrate the discharge box through imperfectly sealed interfaces, and its concentration decreased with argon gas flushing. RH and OH emissions were monitored using a thermohygrometer (Testo 625) and an optical emission spectrometer (Andor Shamrock 500i), respectively. The humidity probe exhibited a measurement accuracy of 0.1% RH. Prior to each experiment, high-purity argon gas was continuously purged into the discharge box. The RH was monitored in real time using the thermohygrometer until it stabilized at 9% RH, after which pulsed RF pattern discharge experiments were initiated.

3. Results and discussion

3.1. The influence of water vapor on the self-organized pattern structure

After igniting a 9.0 MHz pulsed RF discharge, the net RF input power was kept constant at 70 W by adjusting the impedance matching network. Discharge images and pulsed RF voltage waveforms under different RH conditions were simultaneously recorded. Figure 2 shows the temporal characteristics of both the applied RF voltage and corresponding discharge current under operating conditions (10 kHz pulse repetition frequency, 7% duty cycle, 9.1% RH). The inset displays waveforms at the pulse plateau, demonstrating characteristics analogous to those of continuous-wave RF discharges.[25,38] For conciseness, the peak amplitude of the measured pulsed RF voltage is denoted as V_{appl}. The RH dependence of V_{appl} is shown in Fig. 3, revealing a strong correlation between moisture content and discharge behavior. Representative discharge images captured at different RH values are presented in Fig. 4. Notably, at 3.5% RH, optical emission from the OH band in the range of 306.0–312.0 nm confirms the presence of water vapor within the discharge box (see Fig. 5).

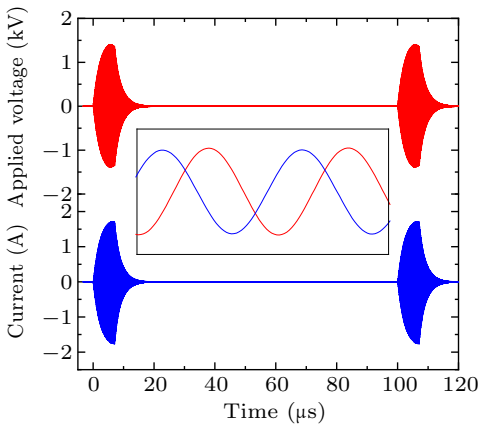


Fig. 2. Pulsed RF applied voltage and discharge current at the pulse repetition frequency of 10 kHz, duty cycle of 7% and RH of 9.1%. Inset shows the voltage (red trace) and current (blue trace) waveforms for the pulse plateau section.

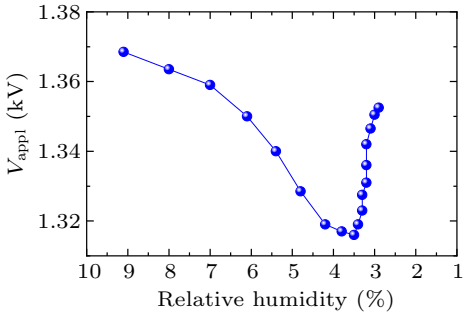


Fig. 3. Amplitude of pulsed RF voltage applied to the electrode as a function of RH. Voltage amplitude is taken at the plateau of the RF pulse. *X*-axis shows RH in decreasing order to highlight the trend under declining humidity conditions.

As the RH decreases, the most noticeable change in Fig. 4 is the progressive transition of discharge coloration from pink through pale pink to white. Significantly, even after achieving full white emission (see Fig. 4(f)), persistent water vapor recycling within the discharge box is confirmed by OH emission spectroscopy (see Fig. 5). Concurrently, both the number of patterns and surface discharge lengths exhibit strong RH dependence between 9.1% and 4.2% RH. Within this range, the pattern count decreases sharply while surface discharge lengths increase substantially, despite maintaining constant discharge power (70 W). Below 4.2% RH (Figs. 4(e)–4(i)), both parameters show gradual evolution, with the pattern count ultimately stabilizing at a minimum of six patterns at 2.9% RH (Fig. 4(i)).

More critically, the structural transformations of patterns demonstrate higher sensitivity to RH variations compared to chromatic evolution and surface discharge length. At the measured highest RH of 9.1% (see Fig. 4(a)), each pattern consists of a central filament and two surface discharges diffused along the dielectric surface. The regions between the surface discharges are dark spaces without gas breakdown. This structure is usually easier to observe in low-frequency DBDs.[7,20,21] When the RH decreases to 6.1%, faint yet uniform side glow discharges emerge between the surface dis-

charges of patterns in the central electrode region. At 4.8% RH, these side glows first become inhomogeneities, with the strongest regions evolving into filaments. In this case, a single pattern consists of a central filament, side glow discharges around the central filament and several side filaments at the boundary.

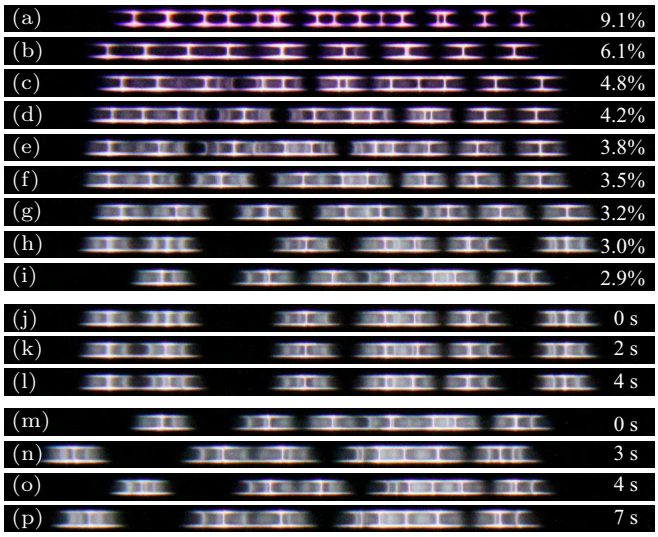


Fig. 4. Discharge images (a)–(i) recorded at different RH; images (j)–(l) and (m)–(p) recorded at RH of 3.0% and 2.9%, respectively, but for different times. In images (j)–(l), the side filaments become unstable, but the central filaments remain motionless; in images (m)–(p), the central and side filaments began moving.

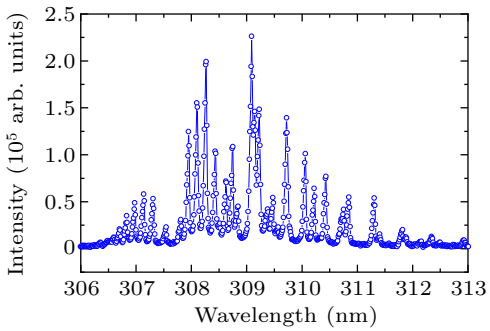


Fig. 5. OH optical emission measured at RH of 3.5%.

When the RH was reduced to 3.5%, the side glow discharges intensified while the number of side filaments diminished. Under these conditions, the structure of the pattern is consistent with that of a 9.0 MHz discharge at different powers (see Fig. 6 in Ref. [35]). Subsequent RH reduction (below 3.5%) yields no further structural reorganization of patterns. Notably, at 3.0% RH the side filaments exhibited slight positional displacement under constant power conditions, while the central filament maintained remarkable stability (see Figs. 4(j)–4(l)). Compared with the discharge image with a RH of 3.0%, when the RH is reduced to 2.9%, although the structure of the pattern does not change significantly, the pattern undergoes random motion as the relative positions of the side filament discharges change, and the discharge image is shown in Figs. 4(m)–4(p).

The influence of water vapor on pulsed RF discharge originates from its characteristics as an electronegative molecular gas. The introduction of water vapor primarily increases both the breakdown and maintenance voltages through enhanced dissociation and electron attachment processes. However, numerical simulations have revealed a non-monotonic relationship between breakdown voltage and water vapor concentration in gas mixtures.[39] The breakdown voltage initially decreases with increasing water vapor content at low concentrations, then rises in higher concentration regimes. Figure 3 shows the relationship between maintenance voltage and RH. However, their dependence is consistent with that of the breakdown voltage on the RH stated above, possibly implying that the breakdown voltage in our pulsed RF discharges also varies monotonically with the water vapor. When the water vapor content is extremely high, the attachment of electrons to water molecules is enhanced, leading to the discharge ignition at a higher voltage. Meanwhile, the discharge maintenance voltage decreases with reducing water vapor content. However, when the water vapor content is lower than a certain value, the increase in water content instead promotes the enhancement of water-related reactions (such as Penning ionization reaction, charge transfer reaction, etc),[39] resulting in the decrease in both breakdown voltage and sustaining voltage with the increase in water vapor.

The structural evolution of patterns is governed by modifications in the side discharge characteristics. A reduction in RH from 9.1% to 3.0% produces pattern structural evolution comparable to that observed when increasing the driving frequency from 3.0 MHz to 9.0 MHz (see Figs. 3, 5 and 6 in Ref. [35]). This analogy extends to the RH-dependent decrease in maintenance voltage, which parallels the frequency-dependent voltage reduction documented in prior work (see Fig. 8 in Ref. [35]). The generation of side discharges requires applied voltages exceeding a critical threshold during the same half-cycles, as supported by both experimental and numerical results.[7,40] In pulsed RF DBDs, side discharges cannot occur during all RF half-cycles, but rather during one of the half-RF cycles when the RF voltage amplitude exceeds a critical value.[35] At 9.1% RH, the RF pulse plateau voltage remains below the side discharge ignition threshold, and therefore no side discharges are generated. When the RH decreases to 6.1%, the concomitant reduction in V_{appl} is offset by a more substantial decrease in breakdown voltage, enabling adjacent RF half-cycle voltages near the pulse plateau to attain the side discharge threshold. With further RH reduction, the continuing decline in RF breakdown and maintenance voltages causes side discharges to transition from diffuse glow to filamentary structures. As discussed above, the reduction in breakdown and maintenance voltages, as well as the generation and evo-

lution of side discharges at this stage, are fundamentally attributed to the weakened electron–water molecule attachment effect caused by the decreasing RH. Notably, at constant V_{appl}, the absorbed power of patterns within identical electrode regions exhibits variations arising from nonuniform distributions of discharge parameters including gas flow, thermal gradients and dielectric surface conditions. These inhomogeneities are manifested as small differences in the structure of the pattern within different electrode regions in the same discharge image.

3.2. Motion of self-organized pattern

At 9.1% RH, self-organized patterns maintain stable morphology without side discharges. When the RH decreases to 6.1%, faint glow mode side discharges emerge but exert negligible influence on central filaments, thereby preserving pattern stability across the electrode regions. As the RH is further reduced from 6.1% to 3.0%, the side filaments shrink from glow to filaments, but the intensity of the side filaments is still very weak, thus maintaining the stability of the pattern. A gradual reduction in RH from 3.0% to 2.9% over 100 min resulted in progressive power attenuation of edge-located patterns due to gas cooling effects, ultimately leading to the extinction of the weakest pattern. Under constant RF power, surviving patterns demonstrate increased power density following pattern number reduction, and the side filaments are enhanced. Notably, spatial or intensity variations in side filaments modulate their electrostatic coupling with the central filament, inducing lateral displacement of the single pattern. This instability triggers collective stochastic motion through nearest-neighbor interactions. To confirm this speculative conclusion, the stability of a single pattern was further investigated.

Figure 6 shows the discharge image of a single pattern under varying RF power at 2.9% RH and 9.0 MHz driving frequency. The annotated power levels represent critical operational thresholds. Figure 6(a) corresponds to the minimum sustaining power threshold, below which immediate discharge extinction occurs. Conversely, Fig. 6(d) indicates the maximum pattern-stable power, beyond which a new pattern will be generated. As the power increases, the pattern structure changes. The side discharge has a uniform glow at low power (Fig. 6(a)), which evolves into non-uniform discharge at medium power (Fig. 6(b)), and unstable filaments at high power (Figs. 6(c) and 6(d)). To quantify RF power effects on side discharge intensity, the radial distribution of the gray value of the pattern in Figs. 6(a)–6(c) is calculated, and the results are shown in Fig. 7. The axial positions are referenced to the midpoint between surface discharges (see the position shown by the red dotted line in Fig. 6(a)). Figure 7 shows that increasing the applied power enhances the side discharge intensity while diminishing the spatial symmetry. In Figs. 6(a)–6(c), the position of the central filament remains almost unchanged, indicating that the pattern is in a quasi-stable state. This quasi-stability ceases and the entire pattern moves randomly with the further increase in power (see Figs. 6(d) and 6(e)). The spatial instability is further demonstrated in the images in Figs. 6(f)–6(j) recorded at different times but at the same power (48 W). In Figs. 6(f)–6(j), those filaments at the two sides of the center filament are not always symmetric with respect to the center (see Fig. 6(h)).

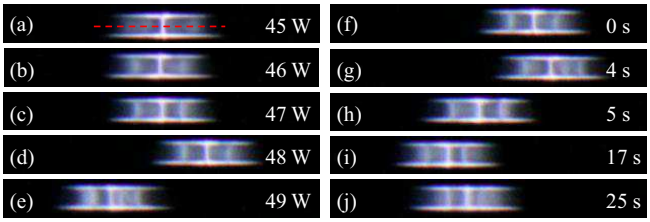


Fig. 6. The 9.0 MHz discharge images of single pattern under different powers ((a)–(e)), and the same power at different times ((f)–(j)), with a RH of 2.9%. Power in images (f)–(j) is constant at 48 W. All power readings in this figure are from the built-in amplifier's digital meter. All images were captured in single shooting mode. Times in images (g)–(j) are referenced to that in image (f).

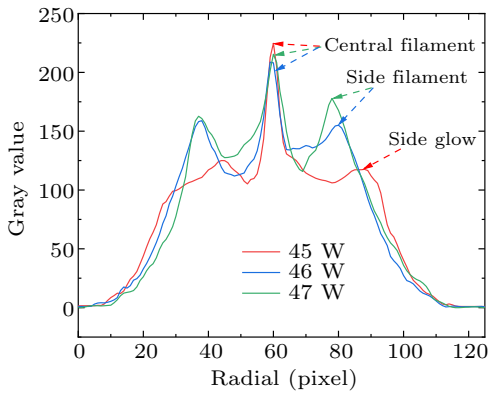


Fig. 7. Radial profiles of gray values of single pattern at different powers. Profiles for 45 W, 46 W and 47 W are calculated from the images in (a)–(c) in Fig. 6. Position of the gray value in the axial calculation is the center of the discharge of the two surfaces of the pattern, and the width is 3 pixels, as shown by the red dotted line in Fig. 6(a).

The preferential reignition mechanism at new spatial locations provides the most plausible explanation for pattern motion in low-frequency DBDs.[41,42] This framework successfully accounts for both vibrating and traveling motion induced by asymmetric filament pairs. While the vibrating motion physical mechanism is well characterized in Ref. [42], its traveling motion counterpart remains less rigorously defined.[41] For the traveling paired filaments that are more closely spaced, the ignition of the weaker filament is more delayed due to the stronger suppression of the electric field of the inverted surface charge deposited by the more intensive filament ignited earlier. Consequently, the weak filament has less time (the breakdown voltage is closer to the maximum of the external applied voltage) to grow before its extinction. As a result, the weaker filament is always weak,

and vice versa. In this case, the interaction between the electric fields of the surface discharge from the two paired filaments always leads to a new reignition in the front of the weak filament and thus the traveling pair.[42]

As described in Section 1, Stollenwerk *et al*. attributed their observed filament motion at high RH to the preferential reignition due to the concentration gradient of water vapor.[23] However, our observations of pattern motion at low RH contradict this proposed mechanism. In pulsed RF discharges, the pattern with the strongest discharge consists of a central filament and several asymmetric side filaments. On the one hand, the pulsed RF pattern resembles low-frequency traveling paired filaments, because the central filament is always stronger than the side filaments surrounding it. On the other hand, the side filaments are located on both sides of the central filament. Crucially, however, side filaments exhibit intrinsic asymmetry governed by localized parameters (e.g., gas gap, surface secondary electron emission coefficients, water vapor concentration). Thus, the resultant motion is directed to the location of the weaker side filament. Furthermore, the varying local conditions can also reverse the location of the weaker side filament in a pattern with respect to the central filament, leading to an unpredictably irregular motion. If the side filaments achieve transient quasi-symmetry over a time interval with respect to the central filament, the pattern remains quasi-static (see Fig. 6(h)). Nevertheless, when the transient quasi-symmetry is destroyed, the pattern again starts to move.

4. Conclusion

In summary, water vapor serves as a critical control parameter governing both structural evolution and stability of self-organized patterns in atmospheric-pressure pulsed RF argon DBDs. Our systematic investigation reveals three distinct operational regimes: (1) at high RH (RH $\geq$ 9.1%), patterns maintain complete stability without side discharge formation; (2) at moderate RH (6.1%–4.8%), uniform glow mode side discharges emerge without compromising pattern stability; (3) below 4.8% RH, side discharges spatially contract from uniform glow to inhomogeneous filamentary structures. The reduction in RH attenuates the electron–water molecule attachment effect, leading to a reduction in the RF breakdown (or maintenance) voltage. Meanwhile, the threshold voltage for igniting side discharges also decreases, which is the fundamental cause of the pattern structure changes. At critically low RH (2.9%), the strongest single pattern undergoes spontaneous motion driven by asymmetric distributions of side filaments, subsequently inducing collective motion across neighboring patterns. The instability originates from the shift of the re-ignition position caused by electrostatic interactions between the center and side filaments. These findings establish water vapor as a pivotal control parameter for tuning pattern structure or stability, providing actionable insights for optimizing pulsed RF DBDs in applications requiring controlled self-organized patterns.

Acknowledgements

This study was partially supported by the Foundation for Innovative Fundamental Research Group Project of Gansu Province (Grant No. 25JRRA805) and the Joint Innovation Fund project of Lanzhou Jiaotong University and Southwest Jiaotong University (Grant No. LH2024023).

References

[1] Chiper A and Borcia G 2013 *Plasma Chem. Plasma Process.* **33** 553
[2] Ran J X, Chen Q Y, Zhou Y X, Tian S, Wu J C, Li P R, Li Q, Zhang X X and Li X C 2025 *Plasma Processes Polym.* **22** e70023
[3] Chauvin J, Judée F, Yousfi M, Vicendo P and Merbahi N 2017 *Sci. Rep.* **7** 4562
[4] Khlyustova A, Labay C, Machala Z, Ginebra M P and Canal C 2019 *Front. Chem. Sci. Eng.* **13** 238
[5] Liao X Y, Liu D H, Xiang Q S, Ahn J, Chen S G, Ye X Q and Ding T 2017 *Food Control* **75** 83
[6] Bourke P, Ziuzina D, Han L, Cullen P J and Gilmore B F 2017 *J. Appl. Microbiol.* **123** 308
[7] Boeuf J P, Bernecker B, Callegari T, Blanco S and Fournier R 2012 *Appl. Phys. Lett.* **100** 244108
[8] Li X C, Ge Y Q, Wan W J, Zhang X X, Sun H, Ran J X, Pang X X, Wu K Y and Jia P Y 2025 *Phys. Scr.* **100** 075602
[9] Fang J L, Zhang Y R, Lu C Z, Gu L L, Xu S F, Guo Y and Shi J J 2024 *Chin. Phys. B* **33** 015201
[10] Liu G M, Chen L, Zhao Z B and Song P 2023 *Chin. Phys. B* **32** 125205
[11] Kogelschatz U 2002 *IEEE Trans. Plasma Sci.* **30** 1400
[12] Han R, Dong L F, Huang J Y, Sun H Y, Liu B B and Mi Y L 2019 *Chin. Phys. B* **28** 075204
[13] Callegari T, Bernecker B and Boeuf J P 2014 *Plasma Sources Sci. Technol.* **23** 054003
[14] Trelles J P 2016 *J. Phys. D: Appl. Phys.* **49** 393002
[15] Brandenburg R 2017 *Plasma Sources Sci. Technol.* **26** 053001
[16] Ouyang J T, Li B, He F and Dai D 2018 *Plasma Sci. Technol* **20** 103002
[17] Dong L F, Zhang L J, He Y N, Wei T, Li Y H, Li C and Pan Y Y 2024 *Appl. Phys. Lett.* **125** 104101
[18] Wu K Y, Wu J C, Jia B Y, Ren C H, Kang P C, Jia P Y and Li X C 2020 *Phys. Plasma* **27** 082308
[19] Qiao Y J, Li B and Ouyang J T 2016 *Phys. Plasma* **23** 013510
[20] Guikema J, Miller N, Niehof J, Klein M and Walhout M 2000 *Phys. Rev. Lett.* **85** 3817
[21] Duan X X, Xu S W, Liu J, He F and Ouyang J T 2011 *IEEE Trans. Plasma Sci.* **39** 2074
[22] Itoh H and Suzuki S 2014 *Plasma Sources Sci. Technol.* **23** 054014
[23] Stollenwerk L, Amiranashvili S and Purwins H G 2006 *New J. Phys.* **8** 217
[24] Zhang Y R, Han Q H, Fang J L, Guo Y and Shi J J 2023 *Chin. Phys. B* **32** 025201
[25] Shi J J, Liu D W and Kong M G 2006 *Appl. Phys. Lett.* **89** 081502
[26] Li B, Chen Q and Liu Z W 2010 *Appl. Phys. Lett.* **96** 041502
[27] Shi J J and Kong M G 2007 *Appl. Phys. Lett.* **90** 111502
[28] Li S, Sun J Z, Sun R, Pan J, Wang L, Chen C, Chen Q and Liu Z W 2022 *Materials* **15** 7647
[29] Yang L Z, Liu Z W, Mao Z G, Li S and Chen Q 2016 *Jpn. J. Appl. Phys.* **56** 01AC02
[30] Li S, Liu Z W, Cai H P and Chen Q 2011 *IEEE Trans. Plasma Sci.* **39** 2134
[31] Balcon N, Aanesland A and Boswell R 2007 *Plasma Sources Sci. Technol.* **16** 217

[32] Shi J J, Zhang J, Qiu G, Walsh J L and Kong M G 2008 *Appl. Phys. Lett.* **93** 041502
[33] Sun J Z, Wang Q, Ding Z F, Li X C and Wang D Z 2011 *Phys. Plasma* **18** 123502
[34] Huo W G, Zhu Y T, Liu C S and Ding Z F 2018 *Phys. Plasma* **25** 093507
[35] Du M Q and Ding Z F 2022 *AIP Adv.* **12** 085217
[36] Liu D W, Shi J J and Kong M G 2007 *Appl. Phys. Lett.* **90** 041502
[37] Zhou W H, Zhang D X, Duan X H, Zhu X, Liu F and Fang Z 2024 *Plasma Sci. Technol.* **26** 094008
[38] Park J, Henins I, Herrmann H W, Selwyn G S and Hicks R F 2001 *J. Appl. Phys.* **89** 20
[39] Lazarou C, Chiper A S, Anastassiou C, Topala I, Mihaila I, Pohoata V and Georghiou G E 2019 *J. Phys. D: Appl. Phys.* **52** 195203
[40] Fan W L, Sheng Z M, Dong L F, Liu F C, Zhong X X, Cui Y Q, Hao F and Du T 2017 *Sci. Rep.* **7** 8368
[41] Brauer I, Bode M, Ammelt E and Purwins H G 2000 *Phys. Rev. Lett.* **84** 4104
[42] Li B, Dong L F, Zhang C, Shen Z K and Zhang X P 2014 *J. Phys. D: Appl. Phys.* **47** 055205